Journal of Inorganic Biochemistry 276 (2026) 113160

Contents lists available at ScienceDirect

Journal of Inorganic Biochemistry

journal homepage: www.elsevier.com/locate/jinorgbio

Targeting non-canonical DNA with *π-extended* Schiff Base complexes of Zinc (II), Copper(II), and Nickel(II): Insights into G-Quadruplex binding modes☆

Luisa D'Anna , Silvia Lo Iacono , Laura Marretta , Simona Rubino , Antonio Palumbo Piccionello , Riccardo Bonsignore *, Giampaolo Barone *

Dipartimento di Scienze e Tecnologie Biologiche, Chimiche e Farmaceutiche, Università degli Studi di Palermo, 90128 Palermo, Italy

A R T I C L E I N F O

Keywords:
G-quadruplex
Metal complexes
Copper
Nickel
Zinc
FRET DNA melting assay

A B S T R A C T

The selective recognition of G-quadruplex (G4) DNA structures by metal complexes holds considerable promise for anticancer drug development, particularly for targeting oncogene promoters and telomeric regions. Herein, we report the synthesis, structural characterization, and DNA-binding strength evaluation of a new series of transition metal complexes derived from a N_4 tetradentate naphthalene-bridged Schiff base ligand (*Naphthim*). The zinc(II), copper(II) and nickel(II) complexes were obtained via in situ or transmetallation protocols and characterized by NMR, HR-ESI-MS, and elemental analysis. Among them, the copper(II) complex, **2**, **[CuNaphthim]** $^{2+}$, exhibited the highest DNA-binding affinity and G4-stabilizing ability, as assessed by FRET-based DNA melting assays, UV–Vis absorption, and circular dichroism (CD) spectroscopy. Despite lacking cationic side chain substituents, **2** showed moderate stabilization of several G4 structures, with a preferential effect on the *cMyc* quadruplex. Comparative studies with the benchmark **[CuPhenim]** $^{2+}$ complex revealed that π-extension of the ligand framework substantially enhances DNA-binding affinity and modulates selectivity.

UV–Vis and CD spectroscopy revealed clear differences in DNA-binding behavior between **2** and **[CuPhenim]** $^{2+}$, with compound **2** exhibiting stronger and more defined interactions across both G4 and duplex targets. These trends found support by molecular docking, which uncovered distinct binding modes depending on G4 topology and echoed the observed affinity profiles. These findings highlight the *Naphthim* scaffold as a promising modular platform for the design of G4-targeting metal complexes.

1. Introduction

G-quadruplexes (G4s) are non-canonical nucleic acid secondary structures characterized by stacked planar guanine tetrads stabilized through Hoogsteen hydrogen bonding. These structures are integral to essential biological processes, including telomere maintenance, transcriptional regulation, and genome stability [1]. Their enrichment in promoter regions of oncogenes—such as *cMyc*, *Bcl2*, and *hTert*—and at telomeric ends, positions them as critical elements in the control of cell proliferation, senescence, and apoptosis [1]. Notably, G4 structures have been implicated in the epigenetic regulation of gene expression, with mounting evidence showing that their stabilization can suppress oncogene transcription and limit uncontrolled growth in tumor cells [2]. This has inspired a growing effort to develop small-molecule G4 binders as precision anticancer therapeutics [1]. Moreover, the selective formation and stability of G4s under cellular stress conditions, particularly in rapidly dividing cells, further enhance their relevance as drug targets. Recent advances in structural biology, including X-ray crystallography and NMR, have shed light on the structural polymorphism of G4s and the diverse conformational states they adopt in physiological contexts, emphasizing the need for binders capable of accommodating this variability [3].

The past decade has witnessed the development of an expanding arsenal of synthetic binders capable of stabilizing G4 with varying degrees of selectivity and potency. These binders are designed to interact through end-stacking on terminal G-quartets, groove binding along the phosphate backbone, or loop-binding that exploits the structural flexibility of the G4 loops [4]. Among these, planar aromatic systems with extended π-conjugation have shown considerable promise for maximizing π–π stacking interactions with the terminal G-tetrads. However,

☆ This article is part of a Special issue entitled: 'MetalsNon-Canonical DNA' published in Journal of Inorganic Biochemistry.

* Corresponding authors.
E-mail addresses: riccardo.bonsignore@unipa.it (R. Bonsignore), Giampaolo.barone@unipa.it (G. Barone).

https://doi.org/10.1016/j.jinorgbio.2025.113160
Received 29 July 2025; Received in revised form 17 November 2025; Accepted 23 November 2025
Available online 30 November 2025

despite these advances, achieving a balance between high binding affinity and structural selectivity remains a key challenge. Electrostatic interactions, hydrogen bonding capacity, and spatial complementarity all influence the binding mode, making binder modularity a valuable asset. Tunable scaffolds, hence, allow chemists to explore how subtle structural changes impact the binding profile, thereby enabling the rational optimization of G4 affinity and selectivity.

In this context, Schiff base ligands have emerged as privileged scaffolds due to their synthetic accessibility and versatile structural motifs [5]. Among these, salphen-type ligands—formed by the condensation of salicylaldehydes with phenylenediamines—have garnered particular attention. These ligands form rigid, planar N_2O_2-donor chelating metals with a high degree of conjugation, and providing an excellent platform for π–π interactions with G4. Their ability to form stable complexes with a variety of metal ions adds further functional diversity.

Transition metal complexes derived from salphen-type ligands offer distinctive advantages for G4 targeting, providing additional handles for tuning geometry, coordination preferences, and compounds' stabilities. The metal center not only modulates the electronic distribution across the ligand framework but also dictates the overall topology of the resulting complex, which can strongly influence DNA-binding affinity and mode [6]. Studies have shown that switching the metal core—from diamagnetic zinc(II) to paramagnetic copper(II) or nickel(II), for instance—can dramatically alter the DNA-binding profile, not only in terms of strength but also in selectivity for particular G4 topologies [7]. Additionally, ligand-centred variations—such as the incorporation of pendant arms, variation of *N^N* bridge substituents, or changes in coordination geometry—can shift the preferred binding site from external stacking to groove or loop binding [8–16]. Collectively, these features endow salphen-like complexes with exceptional structural plasticity, enabling the design of metal-based G4 binders tailored for specific biological targets.

More recently, alternative Schiff base architectures such as the *Phenim* scaffold ((1E,1′E)-*N,N′*-(1,2-phenylene)bis(1-(1*H*-imidazol-4-yl) methanimine) in Fig. 1) have been introduced, replacing the classical bis-salicylidene backbone with a bis(imidazole) motif, endowed with an N_4-donor system. This modification introduces notable changes in both electronics and coordination geometry, while preserving the binder's symmetry and synthetic accessibility. The introduction of imidazole donors confers a softer donor environment and alters the electronic distribution around the metal center, modulating the compound spectroscopic signatures. *Phenim* ligands are capable of supporting a range of transition metal ions and have shown promising results in stabilizing G4 structures, although the observed binding profiles depend strongly on the identity and charge of the central metal and the nature of the G4 topology [7]. Notably, molecular dynamics and spectroscopy studies have suggested that *Phenim*-based copper(II) complex, **[CuPhenim]** $^{2+}$ in Fig. 1, engages in non-classical binding modes, such as loop binding, that may selectively recognize certain G4 topologies over others. These insights underscore the potential of *Phenim*-like scaffolds for fine-tuning DNA interaction profiles through small structural alterations [7]. In a follow up study, **[CuPhenim]** $^{2+}$ has demonstrated a potent anticancer effect on HepG2 cancer cell lines, likely due to the ROS production [17].

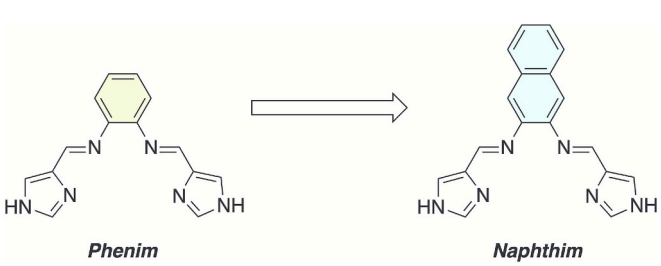

Fig. 1. Molecular structures of the previously reported (left) and newly designed (right) ligands, *Phenim* and *Naphthim*.

Building upon these developments, the current study presents the synthesis and comprehensive characterization of novel zinc(II), copper (II) and nickel(II) complexes featuring naphthalene-based Schiff base ligands (N*aphthim*, ((1E,1′E)-*N,N′*-(2,3-naphthalene)bis(1-(1*H*-imidazol-4-yl)methanimine)). By replacing the phenylene bridge of the *Phenim* system with a more extended and conjugated naphthalene unit, we enhanced the π-surface of the G4 binder while preserving the N_4-donor motif responsible for metal coordination. The use of the *Naphthim* framework not only increases planarity and π-delocalization but also influences the ligand's rigidity and overall three-dimensional topology, factors that are known to modulate DNA-binding modes. This manuscript provides detailed structural analyses through NMR, mass spectrometry, and elemental analysis, alongside biophysical evaluations including UV–Vis binding experiments, FRET melting assays, and circular dichroism spectroscopy. Our findings provide critical insights into ligand-metal interactions, delineating key structure-activity relationships essential for the rational design of next-generation G4-targeting metal complexes. The resulting data not only support the effectiveness of the *Naphthim* platform but also offer broader implications for tuning metal-based molecular recognition of nucleic acid structures.

2. Results and discussion

2.1. Synthesis

The synthesis of zinc(II) and copper(II) complexes (Compounds **1** and **2**, Scheme 1a) was performed in situ by slightly adapting an established protocol previously applied to the parent compound [7]. The Schiff base ligand was synthesized through condensation between equimolar ethanolic solutions of 4-imidazolecarboxaldehyde and 2,3-diaminonaphthalene. Subsequently, 0.5 equivalents of the respective metal perchlorate salt were added, and the mixture was continuously stirred for 24 h. After this period, the desired complexes were collected by filtration as precipitates, yielding high purity products in good yields.

The zinc(II) complex was comprehensively characterized by both ^{1}H and ^{13}C NMR spectroscopy (Figs. S1 and S2). The ^{1}H NMR spectrum revealed resonances consistent with those documented previously for the structurally similar *Phenim* derivative [7]. Specifically, the Schiff base formation was verified by the characteristic resonances observed at approximately 9.4 and 148.8 ppm in the ^{1}H and ^{13}C NMR spectra, respectively. Moreover, the broad resonance around 13.6 ppm observed in the ^{1}H NMR spectrum corresponded to the N*H* imidazolic proton, confirming its retention in the complex. Additionally, the appearance of only six distinct signals in the ^{1}H NMR spectrum affirmed the symmetrical structure of the synthesized complex. This signal distribution is consistent with a C_2-symmetric square-planar zinc(II) coordination environment and confirms that both imidazole arms participate equally in metal binding, ruling out asymmetric binding or partial protonation/deprotonation states.

Due to the intrinsic paramagnetic nature of copper(II), NMR characterization was not feasible for its corresponding complex (**2**). Further structural validation was accomplished through HR-ESI-MS analysis for both **1** and **2** (Figs. S3, S4). Mass spectra exhibited distinct peaks corresponding to the [ML^{2+}] ions, at *m/z* values of 189.0287 for zinc(II) (**1**) and 188.5292 for copper(II) (**2**) complexes (Figs. S3b, S4b). Additionally, a prominent secondary peak, associated with the singly charged species formed via the loss of the imidazolic proton [ML-H^{+}], was detected and aligned well with prior observations for analogous *Phenim* complexes (Figs. S3c, S4c). Interestingly, in contrast to the *Phenim* complex series where the in situ protocol readily produced the nickel(II) complex, analogous attempts to synthesize the nickel(II) N*aphthim* derivative (**3**) under similar conditions consistently yielded inseparable mixtures.

To overcome the synthetic limitations encountered with the in situ approach, a transmetallation strategy was pursued using the zinc(II) complex (**1**) as a reactive intermediate. In the context of the *Naphthim*

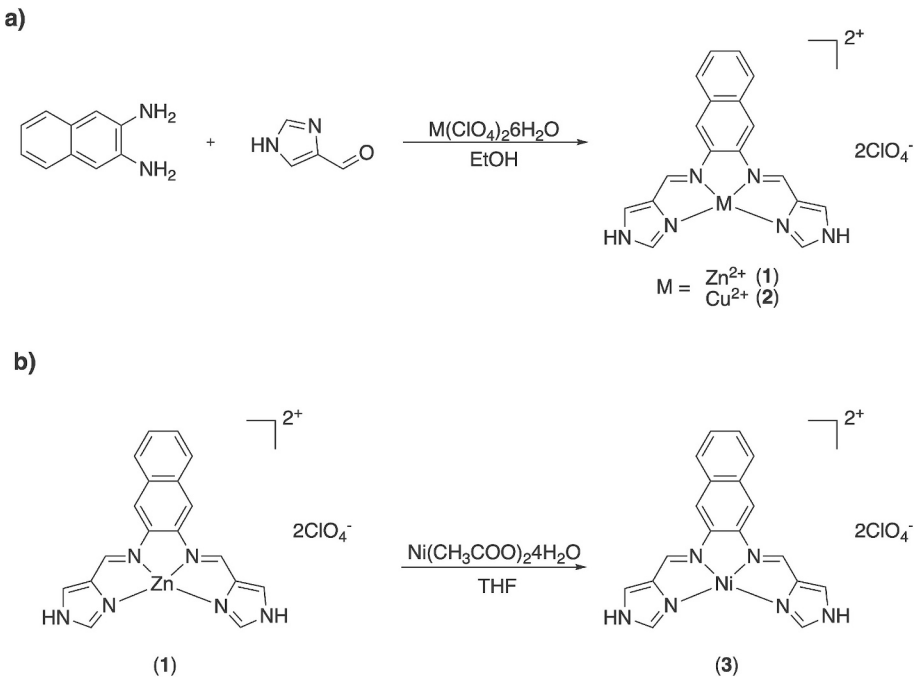

Scheme 1. Synthetic pathway including in situ metal complex formation (a) and transmetallation approach (b).

system, which features a fully aromatic N_4 chelating pocket and embedded imidazolic rings, the use of zinc(II) as a synthetic linchpin offers both electronic stabilization and steric accessibility, enabling post-synthetic metal exchange without compromising the integrity of the conjugated framework. This strategic choice was grounded in the well-documented propensity of zinc(II)-centered salphen-like complexes to act as labile yet structurally preorganized platforms for metal exchange [18,19]. In particular, the zinc(II) ion, characterized by a closed-shell d^{10} configuration and pronounced Lewis acidity, displays a good affinity for oxygen and nitrogen donors yet resulting quite labile. This balance renders zinc(II) complexes kinetically accessible and thermodynamically poised for substitution by more strongly coordinating transition metals such as nickel(II), which form more inert and thermodynamically stable metal complexes [18,20].

Literature precedent, notably from Benet-Buchholz and Kleij [21], supports an associative mechanism wherein a transient heterobimetallic intermediate is formed, allowing stepwise metal displacement via ligand redistribution [22]. This pathway is influenced by both steric and electronic factors within the ligand framework, with more electron-deficient salphen cores enhancing the electrophilicity of the complex and promoting faster transmetallation [21]. In this context, the zinc(II) precursor (**1**) serves not only as a synthetic intermediate but also as a mechanistically rational scaffold that streamlines access to the structurally defined nickel(II) derivative (**3**), overcoming the limitations posed by direct metalation strategies.

Therefore, we decided to prepare a suspension of one equivalent of **1** in tetrahydrofuran, to which an equimolar amount of nickel(II) acetate, previously dissolved in the same solvent, was added. The slurry mixture was stirred at room temperature for 24 h, and the formation of a bright orange precipitate indicated the formation of the desired product. This solid was subsequently isolated by filtration.

Furthermore, the nickel(II) complex exhibited characteristic paramagnetic behavior, resulting in no interpretable NMR signals. Such a result is consistent with previously reported octahedral nickel(II) salphen-type complexes exhibiting $S = 1$ triplet ground states, which typically lead to broadened or entirely suppressed ^1H resonances due to fast relaxation and magnetic anisotropy [7]. This geometry assignment is further supported by the X-ray crystallographic data reported by our group on the structurally related nickel(II) *Phenim* complex, which confirmed a distorted octahedral arrangement consistent with a triplet electronic configuration. The proposed structure was conclusively confirmed via mass spectrometry (Figs. S5), revealing a clear peak at 186.0306 *m/z* corresponding to the [ML^{2+}] species and a second peak at 371.0524 m/z for the [ML-H^+] species. These signals confirm not only the success of the transmetallation but also the preservation of the ligand's protonation state and coordination mode, underscoring the structural robustness of the *Naphthim* scaffold throughout the synthetic sequence.

Final verification of structural integrity and purity for all three complexes was achieved through elemental analysis, demonstrating purities exceeding 99.5 % (see Materials and Methods section).

2.2. DNA binding

To investigate the G-quadruplex (G4) binding properties of the synthesized metal complexes, we employed a fluorescence resonance energy transfer (FRET)-based DNA melting assay. This method is widely recognized for its sensitivity in detecting binder-induced stabilization of nucleic acid secondary structures, particularly G4 motifs. The experimental setup relied on DNA oligonucleotides site-specifically labeled with a FAM donor fluorophore at the 5′ end and a TAMRA acceptor at the 3′ end, enabling real-time monitoring of the thermal unfolding process via fluorescence signal changes. Upon progressive temperature increase, disruption of the folded G4 conformation leads to fluorophore separation and fluorescence enhancement. The temperature at which half of the folded structures are denatured is recorded as the melting temperature (T_m), and any shift in T_m upon addition of a binder (ΔT_m) is taken as a direct indication of structural stabilization.

A screening assay was first carried out on a panel of biologically and structurally diverse G4-forming sequences, including the promoter-associated G4s of *cKit1*, *cKit2*, *Bcl2*, *hTert* and *cMyc*, as well as the telomeric-related sequence hTelo, and a duplex B-DNA (ds-DNA) control. Each oligonucleotide was incubated with the tested metal complexes at a 1:5 DNA-to-binder molar ratio under physiologically relevant buffer conditions. Among the series of compounds, the copper(II) complex **2** exhibited the most appreciable stabilizing effects, with ΔT_m

values of 3.1 °C for *cKit1*, 4.2 °C for *Bcl2*, and 3.3 °C for *cMyc* (Table 1). These values are consistent with moderate G4 stabilization and highlight the capability of **2** to engage structured DNA targets even in the absence of cationic appendages. In contrast, the corresponding nickel(II) and zinc(II) complexes, **1** and **3**, induced minimal thermal shifts across the full sequence panel (Table 1), supporting the hypothesis that copper(II) offers a more favorable balance of coordination geometry and ligand electronic characteristics within the *Naphthim* framework for engaging structured nucleic acid targets.

To further contextualize the performance of **2**, a direct comparative analysis was performed with the benchmark **[CuPhenim]**$^{2+}$. As shown in Fig. 2a, **[CuPhenim]**$^{2+}$ consistently induced higher ΔT_m values across all tested G4 sequences, reflecting its uniform affinity for G4. However, while displaying overall lower ΔT_m values than the benchmark, **2** surpassed by a few degrees **[CuPhenim]**$^{2+}$ specifically on the *cMyc* G4. This distinctive profile suggests that subtle variations in the metal complex framework — such as the more extended aromatic surface and altered electronic distribution of the *Naphthim* scaffold — may selectively enhance interactions with the structural features of particular G4 topologies. This sequence-selective behavior — especially the preferential stabilization of *cMyc* — aligns with the broader goal of developing binders capable of targeting regulatory quadruplex structures with high precision.

To explore this further, concentration-dependent FRET melting experiments were performed on **2**'s most responsive targets, *Bcl2* and *cMyc*, using a range of complex concentrations from 0.5 to 20 equivalents. The resulting thermal profiles, reported in Fig. 2b, revealed an interesting pattern. For *Bcl2*, thermal stabilization rose up to 1 equivalent of **2** and then remained constant within the experimental error, suggesting that binding saturation is reached under these conditions. In contrast, ΔT_m values for *cMyc* continued to increase beyond 5 equivalents without clear signs of plateauing, indicating that the interaction is still responsive to additional binder. These differing trends support the view that **2** interacts with G4 structures in a sequence-dependent manner, with the *Bcl2* G4 forming a well-defined binding interface that saturates quickly, while *cMyc* exhibits a more progressive response to increasing concentrations. Taken together, the data suggest that **2** engages the two G4s via different binding modes: the rapid saturation observed with *Bcl2* could be consistent with a discrete, well-defined site in a groove or in a loop, whereas the gradual increase observed with *cMyc* implies a more accessible and potentially less structurally restricted binding region. Hence, the existence of two distinct binding modes for the copper(II) complex and the two different G4s can reasonably be proposed based on these experimental differences.

To complement the FRET-based findings with a spectroscopic perspective, UV–Vis DNA Binding studies of the copper(II) complexes **2** and **[CuPhenim]**$^{2+}$ were next performed in buffered aqueous solution. Notably, the electronic absorption spectrum of **2**, featuring the more extended π-conjugated Naphthim core, displays a single broad absorption band centered at 337 nm. This contrasts with **[CuPhenim]**$^{2+}$, which exhibits two partially resolved bands at 314 and 347 nm. Such differences in spectral profiles underscore distinct electronic structures in these two complexes, as previously noted for structurally related Schiff base copper(II) systems [7]. These spectral features thus provide useful markers for subsequent DNA interaction studies.

In order to investigate the DNA-binding affinity of the copper(II) complexes **2** and **[CuPhenim]**$^{2+}$, UV–Vis absorption experiments were performed by adding increasing amounts of DNA sequences to the two metal complexes. In particular, calf thymus DNA (Ct-DNA) was chosen as a model for duplex B-form DNA, while *Bcl2* and *cMyc* G-quadruplex-forming sequences were selected according to the FRET DNA melting results (see Fig. 3). To minimize spectral interference from the nucleic acid absorption near 260 nm, the DNA-binding was monitored by exploiting solely the absorption bands at 337 nm (**2**) and 347 nm (**[CuPhenim]**$^{2+}$) of the complexes. Although the interaction of **[CuPhenim]**$^{2+}$ with Ct-DNA and *cMyc* had been previously reported [7], these experiments were repeated under the current buffer conditions, as ionic strength is known to strongly affect nucleic acid recognition by small molecules [23].

For **2**, the absorption maximum at 337 nm red-shifted markedly with increasing DNA equivalents, while sharp and persistent isosbestic points were observed throughout the experiments, indicating an equilibrium between the free metal complex and the DNA-bound one. In contrast, DNA-binding analysis with **[CuPhenim]**$^{2+}$ resulted in more modest red shifts and less well-defined isosbestic points, suggesting a weaker interaction.

To quantify these observations, in particular to achieve a consistent comparison among the investigated metal complexes, binding constants (K_b) were calculated by fitting the absorption changes according to literature known protocols [24,25]. Importantly, compared to linear fitting methods [26], this approach does not introduce overestimation of the binding constants, as recently highlighted [27]. The analysis of their values, reported in Table 2, revealed that **2** binds all three DNA sequences more tightly than **[CuPhenim]**$^{2+}$, with differences ranging from one to nearly two orders of magnitude. In particular, for *Bcl2* and *cMyc*, **2** displayed K_b values approximately 10-fold higher than its *Phenim* analogue, confirming its enhanced ability to engage G4s. While a direct comparison between different techniques is not ideal, it should be noted that the similar affinity of **2** observed for *Bcl2* and *cMyc* mirrors the trend observed in FRET melting experiments.

However, the most striking difference emerged in the binding to Ct-DNA. While **[CuPhenim]**$^{2+}$ exhibited a similar affinity for the duplex target than G4, **2** bound Ct-DNA even more tightly than either of the G4s, reaching K_b values in the 10^6 M^{-1} range: this resulted in an overall difference of nearly two orders of magnitude in Ct-DNA binding between the two copper(II) complexes, **2** and **[CuPhenim]**$^{2+}$. Such a profile indicates that **2** is capable of engaging both canonical and non-canonical DNA topologies with high efficiency, likely due to its extended aromatic surface and planar coordination geometry, which may facilitate stacking or groove-binding interactions across multiple DNA forms.

To probe whether such interactions are purely affinity-driven or also induce conformational consequences, we next turned to circular dichroism (CD) spectroscopy to assess potential structural changes in duplex DNA upon binding. Under the tested buffer conditions, calf thymus DNA (Ct-DNA) exhibits a canonical B-form CD spectrum, characterized by a strong positive band at about 275 nm and a negative band at ca. 245 nm, both of which are associated with right-handed helicity and base stacking interactions. These signals provide a reliable baseline for monitoring binder-induced alterations.

Upon addition of increasing equivalents of **2** clear perturbations to Ct-DNA signature emerged, with a notable decrease in the positive band intensity. More importantly, the copper(II) complex presence resulted in the appearance of induced CD (ICD) bands matching the complex's UV–Vis absorption range (see inset in Fig. 4a). The emergence of these

Table 1
ΔT_m values and associated errors of 0.2 μM Ds- and G4-DNAs upon interaction with metal complexes at 1 μM concentration.

Complex	Ds-DNA	*cKit1*	*cKit2*	*Bcl2*	*hTert*	*hTelo*	*cMyc*
1	0.4 ± 1.3	0.6 ± 0.1	0.5 ± 0.4	0.8 ± 0.1	0.6 ± 0.2	1.1 ± 0.1	2.1 ± 2.7
2	0.4 ± 0.3	3.1 ± 0.5	2.9 ± 0.1	4.2 ± 0.8	2.9 ± 0.6	2.8 ± 0.1	3.3 ± 0.2
3	0.1 ± 0.1	2.2 ± 0.8	1.1 ± 0.6	1.2 ± 0.7	0.7 ± 0.1	2.1 ± 0.4	0.5 ± 0.3
[Cu-Phenim]$^{2+}$	1.5 ± 0.7	8.9 ± 2.1	3.4 ± 0.4	6.7 ± 0.2	3.7 ± 0.4	1.7 ± 0.1	0.3 ± 0.4

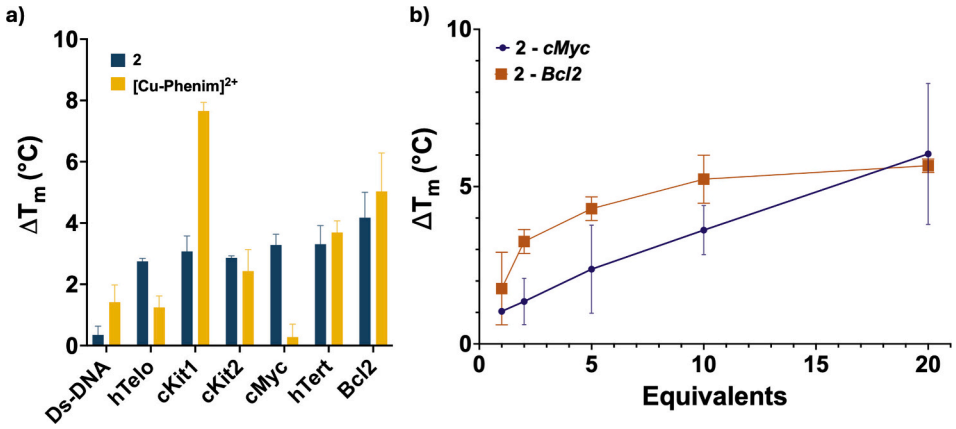

Fig. 2. a) ΔT_m values of different G4-DNAs and Ds-DNA in the presence of 5 equivalents of either **2** or **[CuPhenim]** $^{2+}$. b) ΔT_m values of *cMyc* and *Bcl2* G4s in the presence of increasing equivalents of **2**.

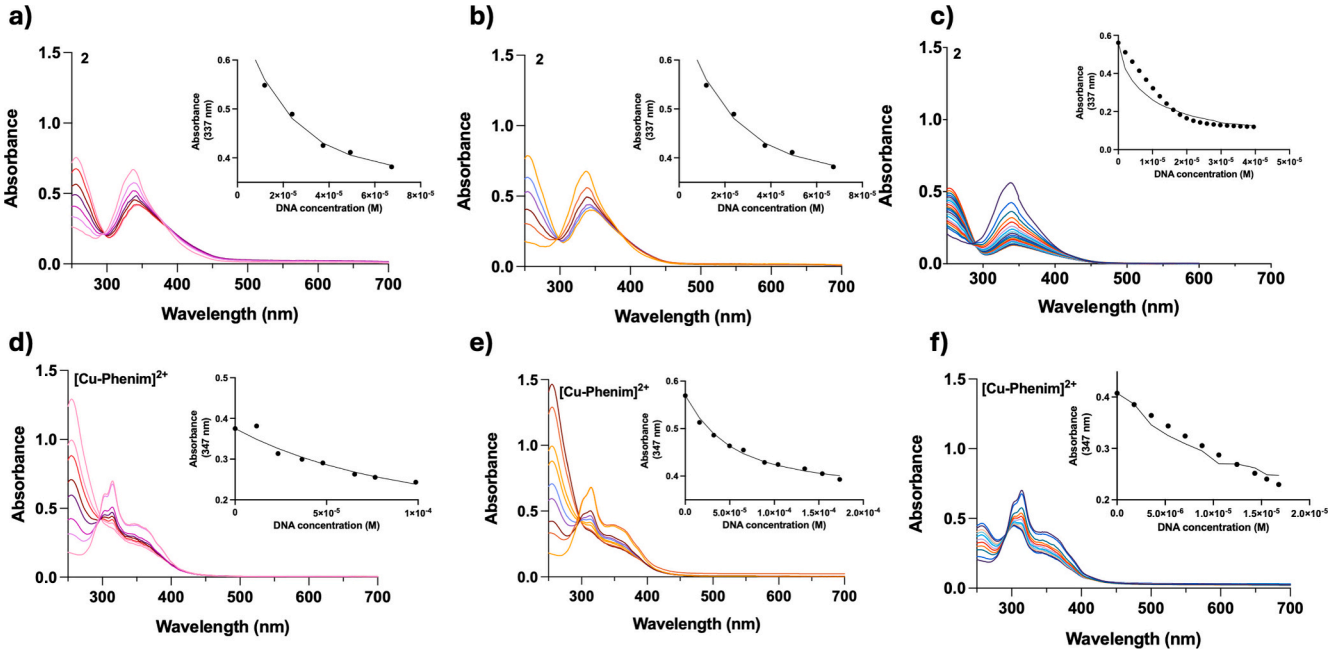

Fig. 3. UV–Vis absorption spectrum of **2** (a-c) and **[CuPhenim]** $^{2+}$(d-f) in combination with increasing amount of *cMyc* (a-d), *Bcl2* (b,e) G4s and Ct-DNA (c,f). Concentration of DNA is reported in bases. (a) [**2**] = 21.5 μM, [*cMyc*] = 0–74.8 μM; (b) [**2**] = 21.9 μM, [*Bcl2*] = 0–67.3 μM; (c) [**2**] = 17.9 μM, [Ct-DNA] = 0–39.56 μM. (d) **[CuPhenim]** $^{2+}$ = 24.9 μM, [*cMyc*] = 0–98.7 μM; (e) **[CuPhenim]** $^{2+}$ = 24.0 μM, [*Bcl2*] = 0–154.0 μM; (f) **[CuPhenim]** $^{2+}$ = 25.7 μM, [Ct-DNA] = 0–16.8 μM. In the inset, representative data fitting.

Table 2
K_b values calculated by UV–Vis experiments.

Complex	Ct-DNA	*Bcl2*	*cMyc*
2	(16.50 ± 0.01) * 10^5	(1.17 ± 0.03) * 10^5	(1.22 ± 0.02) * 10^5
[Cu-Phenim] $^{2+}$	(0.70 ± 0.02) * 10^5	(0.28 ± 0.02) * 10^5	(0.11 ± 0.03) * 10^5

ICD signals strongly supports a chiral environment-induced ordering of **2** — consistent with its well-defined orientation along the DNA groove or within its base stack. Such behavior is typically associated with groove binding or partial intercalation, rather than mere electrostatic association. By contrast, **[CuPhenim]** $^{2+}$ elicited far subtler changes in the CD spectrum, with the B-form features largely preserved and only negligible ICD signals emerging, consistent with a weaker mode of interaction. The more profound spectral changes seen with **2**, hence, point toward a different binding paradigm, likely facilitated by its more extended π-conjugation and planar coordination framework. Similar CD measurements performed on the G4-forming sequences *Bcl2* and *cMyc* (Fig. S7) showed only minor spectral perturbations by the two metal complexes. The absence of appreciable ICD bands in the presence of G4-DNA, together with their clear appearance in the **2**–Ct-DNA solutions, is consistent with the tighter and more ordered binding interaction of **2** with the duplex DNA, observed through UV–Vis absorption measurements.

In an effort to gain deeper insights into the experimental UV–Vis and FRET observations, molecular docking studies were performed with compound **2** and **[CuPhenim]** $^{2+}$ targeting the *Bcl2* and *cMyc* G4s. The docking outcomes revealed distinct and intriguing binding preferences that align closely with the observed experimental behaviors (Fig. 5 and Fig. S8).

For the *Bcl2* G4 structure, **2** notably adopts an unconventional groove-binding mode, interacting intimately within the G4 grooves

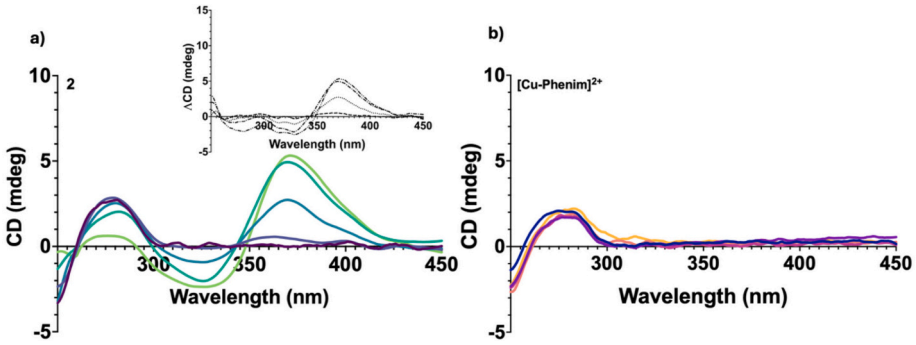

Fig. 4. CD spectra of Ct-DNA in the presence of increasing aliquots of **2** and **[CuPhenim]** $^{2+}$. Tris-HCl 50 mM, KCl 100 mM, pH = 7.4. a) [Ct-DNA] = 21.9 μM, [**2**] = 0–67.3 μM; b) [Ct-DNA] = 37.8 μM, **[CuPhenim]** $^{2+}$ = 0–45.0 μM. In the inset, variations of the DNA-CD signals recorded in the presence of increasing amounts of **2**.

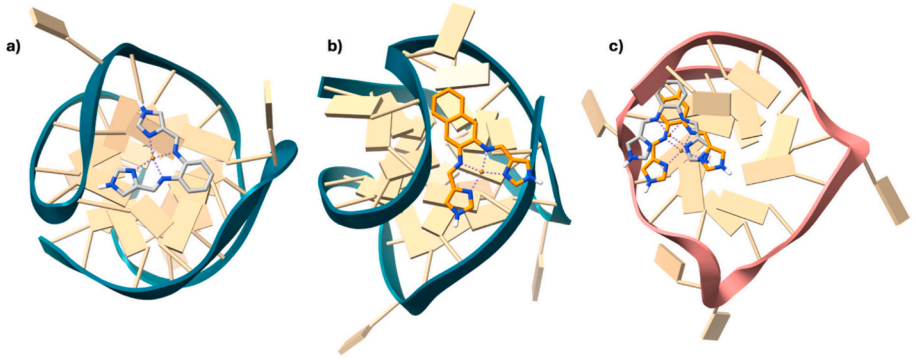

Fig. 5. Cartoons showing top view possible binding sites of (a) **[CuNaphthim]** $^{2+}$ (**2**) (Orange) and **[CuPhenim]** $^{2+}$ (Grey) with *Bcl2* G4 (PDB id: 6ZX7) and (b) of **[CuNaphthim]** $^{2+}$ (Orange) and **[CuPhenim]** $^{2+}$ (Grey) *cMyc* (PDB id: 2LBY) G4 motifs. Side views are shown in the ESI.

rather than engaging the terminal guanine tetrads directly. This distinctive groove-binding mode, visualized clearly in the docking pose (orange coloured compound in Fig. 5a and S7), could plausibly explain the rapid saturation observed in the FRET melting assays, indicating a defined and potentially constrained binding interface. By contrast, the structurally related complex **[CuPhenim]** $^{2+}$ demonstrates the classical end-stacking mode, effectively sandwiching itself onto the planar G-quartets, as expected from its rigid planar geometry (grey coloured molecule in Fig. 5a,c and S8). This juxtaposition not only highlights the influence of subtle ligand modifications on binding orientation but also underscores how structural flexibility can open alternative binding pathways.

Turning to the *cMyc* G4 (Fig. 5c and S8), both complexes show a preference for the traditional top-stacking interaction, positioning themselves squarely atop the terminal guanine tetrads. This binding mode corroborates well with the gradual stabilization profile captured in FRET experiments, suggestive of a broader and more accessible binding surface on *cMyc* compared to *Bcl2*.

While docking scores for metal-based complexes must be interpreted with caution—owing to the limitations of most scoring functions in accurately capturing metal coordination and electronic effects [28]—they nonetheless reflect a consistent and meaningful trend. In both G4 systems, compound **2** yields more favorable docking scores than **[CuPhenim]** $^{2+}$, with values of −6.24 and − 5.54 kcal·mol^{-1} for *Bcl2* and *cMyc*, respectively, compared to −4.90 and − 4.84 kcal·mol^{-1} for the *Phenim*-based reference. This trend compellingly echoes the outcome of the UV–Vis binding studies, which revealed stronger affinities for **2** across all targets.

The convergence of computational and spectroscopic data strengthens the proposed binding models: in this context, the copper(II) complex, **2**, emerges as a structurally adaptable ligand capable of optimizing its binding mode to exploit distinct topological features in different G4 (and Ds-DNA) targets—a feature that may underpin its selective stabilization behavior observed experimentally.

Conclusions. The present work underscores the potential of naphthalene-bridged Schiff base ligands (N*aphthim*) as a versatile scaffold for the development of metal-based DNA binders capable of engaging both canonical and non-canonical nucleic acid structures. Through the synthesis and comprehensive spectroscopic evaluation of zinc(II), copper(II), and nickel(II) complexes derived from this expanded π-conjugated ligand, we demonstrate how subtle structural modifications can fine-tune both affinity and mode of DNA interaction. Among the series, the **[CuNaphthim]** $^{2+}$ complex, **2**, stood out for its consistently higher binding affinities and G4-stabilizing properties, despite the absence of cationic substituents or appended side chains.

While **2** does not display pronounced selectivity for G-quadruplexes over duplex DNA under the tested conditions, its capacity to stabilize select G4 structures—most notably the oncogenic *cMyc* motif—more effectively than the benchmark **[CuPhenim]** $^{2+}$, suggests that ligand topology and electronic tuning alone can impart a degree of sequence responsiveness.

Molecular docking provided additional mechanistic insights, revealing that **2** adopts differentiated binding modes depending on the topology of the G4 target. A groove-binding orientation was observed with the *Bcl2* G4, consistent with rapid saturation in FRET melting assays, while a conventional terminal stacking mode was favored in the interaction with *cMyc*. Notably, the observed docking score trends mirrored the experimental UV–Vis binding constants, reinforcing the hypothesis that π-extension and increased planarity in the ligand scaffold enhance both DNA affinity and topological adaptability. Although the absolute accuracy of docking energies for transition metal complexes remains limited, the convergence of computational and spectroscopic data lends credence to these structural models.

Collectively, these findings reveal how minor yet strategic changes in

ligand design—such as the shift from a phenylene to a naphthalene bridge—can profoundly reshape the DNA-binding behavior of copper(II) complexes. The differentiated interaction profiles observed for **[CuNaphthim]** $^{2+}$ not only provide a structural rationale for its experimental performance but also offer valuable design principles for next-generation G4-targeting agents. Looking ahead, further derivatization of the *Naphthim* platform, along with redox activity studies and cellular assays, will be essential to fully explore its potential as a modular core for metal-based therapeutics. In particular, modifications at the aldehydic positions—such as the introduction of positively charged side chains—may enhance aqueous solubility and electrostatic attraction toward the negatively charged DNA backbone, potentially increasing both affinity and selectivity for G4 structures. This strategy, already successful in classical salphen systems, could be adapted to the *Naphthim* scaffold to synergistically combine π-stacking capability with backbone anchoring, opening avenues for the design of highly efficient G4 stabilizers.

3. Experimental procedures

3.1. Synthesis

Compounds **1** and **2** were synthesized by dissolving 0.50 mmol of 2,3 diaminonaphthalene in ethanol, followed by the dropwise addition of 1.00 mmol of 4-imidazolecarboxaldehyde under continuous stirring. After the complete addition of the aldehyde, 0.50 mmol of the appropriate metal salt (Zn^{2+} for compound **1** or Cu^{2+} for compound **2**) was added to the reaction mixture. The resulting solution was stirred at room temperature for 24 h using a magnetic stirrer.

After the reaction period, the formation of a solid precipitate was observed in both cases and collected after filtration. The crude products were washed successively with cold diethyl ether, ethanol and water to remove residual impurities. The resulting solids were dried under vacuum and used without further purification.

To obtain compound **3**, 0.14 mmol of compound **1** were dissolved in 15 mL of tetrahydrofuran (THF). To this solution, 0.15 mmol of nickel (II) acetate, pre-dissolved in 7 mL of THF, was added and stirred at room temperature for 24 h. Following the reaction period, a precipitate was observed and collected by filtration. The solid was then washed sequentially with distilled water, cold methanol, ethanol, and diethyl ether. The final product, obtained as an orange solid, was dried under vacuum prior to further analysis.

Compound 1. ^{1}H NMR (400 MHz, DMSO-d_6) δ 13.58 (s, 1H), 9.44 (s, 1H), 8.62 (s, 1H), 8.57 (s, 1H), 8.26 (s, 1H), 8.01 (dd, J = 6.2, 3.3 Hz, 1H), 7.64 (dt, J = 6.3, 3.4 Hz, 1H).

^{13}C NMR (101 MHz, DMSO) δ 148.84, 139.22, 136.12, 135.21, 132.62, 128.45, 127.68, 124.37, 116.11.

ESI-MS Expected for [ML^{2+}]: 189.0286; found 189.0287.

Elemental analysis of $C_{18}H_{14}Cl_2N_6O_8Zn$ (**1**): Calculated: C 37.36 %, H 2.44 %, N 14.52 %. Found: C 36.97 %, H 2.63 %, N 14.26 %.

Compound 2. ESI-MS Expected for [ML^{2+}]: 188.5281; found 188.5292.

Elemental analysis of $C_{18}H_{16}Cl_2N_6O_9Cu$ (**2•H_2O**): Calculated: C 36.35 %, H 2.71 %, N 14.13 %. Found: C 36.50 %, H 2.66 %, N 13.82 %.

Compound 3. ESI-MS Expected for [ML^{2+}]: 186.0306; found 186.0326.

Elemental analysis of $C_{18}H_{16}Cl_2N_6O_9Ni$ (**3•H_2O**): Calculated: C 36.65 %, H 2.73 %, N 14.25 %. Found: C 36.80 %, H 2.86 %, N 13.9 %.

3.2. FRET DNA melting assay

To evaluate the G4 stabilizing capabilities of the synthesized complexes, a FRET-based DNA melting assay was employed. This technique assesses the thermal stability of a labeled oligonucleotide sequence bearing two fluorophores—typically FAM at the 5′ end and TAMRA at the 3′ end. In such a configuration, FAM emits fluorescence at a wavelength absorbed by TAMRA. When the G4 structure is intact, the fluorophores remain in proximity, resulting in efficient fluorescence resonance energy transfer (FRET) and quenching of the FAM signal. Upon gradual heating of the solution, the hydrogen bonds stabilizing the G-quartets are disrupted, causing the oligonucleotide to unfold and increasing the spatial separation between the fluorophores. This leads to a reduction in FRET efficiency and a concomitant rise in the detectable FAM fluorescence signal.

The oligodeoxynucleotides (ODNs) were diluted to the desired concentrations using a 60 mM or 10 mM (+ 50 mM LiCl) potassium cacodylate buffer (pH 7.4). To induce folding into either B-DNA or G4 topologies, the solutions were heated to 95 °C for 5 min, followed by gradual cooling to room temperature overnight. In the final assay mixtures, the ODN concentration was adjusted to 0.2 μM in a total volume of 30 μL. The metal complexes were initially dissolved in DMSO to prepare 1 mM stock solutions and subsequently diluted with buffer, ensuring that the final DMSO concentration did not exceed 0.1 %.

3.3. UV–Vis and Circular dichroism

UV–Vis absorption spectra were recorded at room temperature using a Cary 1E double-beam spectrophotometer. Experiments were performed by gradually adding increasing amounts of G4-DNA or B-DNA to a solution of metal complexes **2** and **[CuPhenim]** $^{2+}$ at constant concentration. To ensure that the concentration of each metal complex remained unchanged throughout the assay, an equal volume of a double-concentrated metal complex solution was added simultaneously with each DNA addition. Binding constants (K_b) were obtained fitting the UV–Vis titration data at 337 (**2**) and 347 nm (**[CuPhenim]** $^{2+}$) by means of the following equation [24,25].

$$Abs = \left\{ \varepsilon_f \frac{\varepsilon_b b K_b [DNA]}{1 + 0.5\left\{ -(1 - K_b[B] + K_b[DNA]) + \sqrt{(1 - K_b[B] + K_b[DNA])^2 + 4K_b[B]} \right\}} \right\} \times \frac{-\left(1 - K_b[B] + K_b[DNA] + \sqrt{(1 - K_b[B] + K_b[DNA])^2 + 4K_b[B]}\right)}{2K_b}$$

where [B] is the concentration of the complexes used during the experiments, $\varepsilon_a = Abs_{observed}/[B]$, ε_b is the extinction coefficient of the DNA-bound complex, treated as a free variable and optimized together with K_b by minimizing the global residual error across the entire titration dataset, ε_f is the extinction coefficient of the free complex determined by a calibration curve, following the Beer–Lambert law, and b is the path length.

The compounds were initially dissolved in dimethyl sulfoxide

(DMSO) and subsequently diluted with the titration buffer, consisting of 10 mM Tris-HCl supplemented with 50 mM KCl.

CD spectra were recorded using a Jasco J-715 spectropolarimeter at 25 °C. Increasing amounts of metal complexes **2** and **[CuPhenim]** $^{2+}$ were added into a DNA solution maintained at constant concentration. Experimental parameters were as follows: wavelength range 450–220 nm, response time 0.5 s, 4 accumulations, and a scanning speed of 200 nm/min.

ODNs and Ct-DNA were dissolved in Tris–KCl buffer (50 mM Tris–HCl, 100 mM KCl, pH 7.4) to obtain 100 μM stock solutions, expressed in monomer units. G4 folding was performed as described in the FRET analysis section. To ensure that the concentration of *ODNs or Ct-DNA* remained unchanged throughout the assay, an equal volume of a double-concentrated DNA or ODN solution was added simultaneously with each addition of metal complex solution.

3.4. Docking calculations

The structures of the metal complexes were fully optimized using Density Functional Theory (DFT) as implemented in the Gaussian16 software package [29]. The B3LYP functional was employed in combination with the CEP-121G pseudopotential basis set for the metal centers, and the 6-311G(d,p) basis set for all remaining atoms.

Receptor structures for *Bcl2* (PDB ID: 6ZX7) and *cMyc* (PDB ID: 2LBY), along with the optimized metal complexes, were prepared for docking using AutoDock Tools 1.5.6 [30]. The systems were converted into the required PDBQT format. Blind-docking was performed by generating sufficiently large grid boxes to encompass all potential binding regions of the receptors. Specifically, for Bcl2 (6ZX7), the grid dimensions were set to 60 × 70 × 56 points with a spacing of 0.375 Å, and centered at coordinates x = −0.736, y = 0.513, z = −3.276. For cMyc (2LBY), the grid was defined as 56 × 52 × 54 points with the same grid spacing, and centered at x = −0.273, y = −0.037, z = −0.135. All molecular visualizations were generated using ChimeraX [31].

Docking calculations were carried out using AutoDock 4.2 [30], employing the Lamarckian Genetic Algorithm. All docking parameters were kept at their default values unless otherwise specified. The predicted binding affinities are reported as estimated free energies of binding in kcal·mol^{-1}.

CRediT authorship contribution statement

Luisa D'Anna: Writing – original draft, Validation, Methodology, Investigation, Formal analysis. **Silvia Lo Iacono:** Methodology, Investigation, Formal analysis. **Laura Marretta:** Investigation, Formal analysis. **Simona Rubino:** Formal analysis. **Antonio Palumbo Piccionello:** Formal analysis. **Riccardo Bonsignore:** Writing – review & editing, Writing – original draft, Supervision, Funding acquisition, Conceptualization. **Giampaolo Barone:** Writing – review & editing, Writing – original draft, Supervision, Funding acquisition, Conceptualization.

Declaration of competing interest

The authors declare that they have no known competing financial interests or personal relationships that could have appeared to influence the work reported in this paper.

Acknowledgements

RB and LD acknowledge financial support under the PRIN D.D. 104/2022 PNRR M4.C2.1.1. – Project Code: 2022AN47CA – CUP: B53D23013590001, funded by the European Union – NextGenerationEU– Project Title "La-G4-DACA" – Grant Assignment DD 862, 16/06/2023. GB thanks for financial support the European Union – NextGenerationEU through the Italian Ministry of University and Research under PNRR - M4C2-I1.3 Project PE_00000019 "HEAL ITALIA" CUP: B73C22001250006 and the PRIN2022 D.D. 20432/2024-PE5 Project Code: 2022APCTNA – CUP: I53C24002220006, funded by the European Union – NextGenerationEU– Project Title "TRILLI".

Appendix A. Supplementary data

Supplementary data to this article can be found online at https://doi.org/10.1016/j.jinorgbio.2025.113160.

References

[1] P. Pramanik, S. Bhattacharya, Decoding the prospective of metal complexes in anti-Cancer therapeutics by targeting of G-Quadruplex DNA, J. Inorg. Biochem. 270 (2025) 112947, https://doi.org/10.1016/j.jinorgbio.2025.112947.
[2] K. Sato, P. Knipscheer, G-Quadruplex resolution: from molecular mechanisms to physiological relevance, DNA Repair 130 (2023) 103552, https://doi.org/10.1016/j.dnarep.2023.103552.
[3] T.D. Prieto Otoya, K.T. McQuaid, C.J. Cardin, Structural insights into G-Quadruplex binding by metal complexes: implications for drug design, Med. Chem. Res. 33 (11) (2024) 2001–2019, https://doi.org/10.1007/s00044-024-03309-w.
[4] M.P. O'Hagan, J.C. Morales, M.C. Galan, Binding and beyond: what Else can G-Quadruplex ligands do? Eur. J. Org. Chem. 2019 (31−32) (2019) 4995–5017, https://doi.org/10.1002/ejoc.201900692.
[5] L. D'Anna, L. Marretta, A. Froux, S. Rubino, V. Butera, A. Spinello, R. Bonsignore, A. Terenzi, G. Barone, DNA binding activity of functionalized Schiff Base metal complexes, Eur. J. Inorg. Chem. 28 (6) (2025), https://doi.org/10.1002/ejic.202400705.
[6] R. Bonsignore, E. Trippodo, R. Di Gesù, A.P. Carreca, S. Rubino, A. Spinello, A. Terenzi, G. Barone, Novel half Salphen cobalt(III) complexes: synthesis, DNA binding and anticancer studies, Dalton Trans. 53 (14) (2024) 6311–6322, https://doi.org/10.1039/D4DT00092G.
[7] G. Farine, C. Migliore, A. Terenzi, F. Lo Celso, A. Santoro, G. Bruno, R. Bonsignore, G. Barone, On the G-Quadruplex binding of a new class of nickel(II), copper(II), and zinc(II) Salphen-like complexes, Eur. J. Inorg. Chem. 2021 (14) (2021) 1332–1336, https://doi.org/10.1002/ejic.202100067.
[8] N.H. Campbell, N.H.A. Karim, G.N. Parkinson, M. Gunaratnam, V. Petrucci, A. K. Todd, R. Vilar, S. Neidle, Molecular basis of structure–activity relationships between Salphen metal complexes and human telomeric DNA quadruplexes, J. Med. Chem. 55 (1) (2012) 209–222, https://doi.org/10.1021/jm201140v.
[9] R. Bonsignore, F. Russo, A. Terenzi, A. Spinello, A. Lauria, G. Gennaro, A. M. Almerico, B.K. Keppler, G. Barone, The interaction of Schiff Base complexes of nickel(II) and zinc(II) with duplex and G-Quadruplex DNA, J. Inorg. Biochem. 178 (2018) 106–114, https://doi.org/10.1016/j.jinorgbio.2017.10.010.
[10] L. Sabater, M.-L. Nicolau-Travers, A. De Rache, E. Prado, J. Dejeu, O. Bombarde, J. Lacroix, P. Calsou, E. Defrancq, J.-L. Mergny, D. Gomez, G. Pratviel, The nickel (II) complex of Guanidinium phenyl porphyrin, a specific G-Quadruplex ligand, targets telomeres and leads to POT1 Mislocalization in culture cells, J. Biol. Inorg. Chem. 20 (4) (2015) 729–738, https://doi.org/10.1007/s00775-015-1260-8.
[11] A. Terenzi, D. Lötsch, S. van Schoonhoven, A. Roller, C.R. Kowol, W. Berger, B. K. Keppler, G. Barone, Another step toward DNA selective targeting: Ni ^{II} and Cu ^{II} complexes of a Schiff Base ligand able to bind gene promoter G-Quadruplexes, Dalton Trans. 45 (18) (2016) 7758–7767, https://doi.org/10.1039/C6DT00648E.
[12] A. Terenzi, R. Bonsignore, A. Spinello, C. Gentile, A. Martorana, C. Ducani, B. Högberg, A.M. Almerico, A. Lauria, G. Barone, Selective G-Quadruplex stabilizers: Schiff-Base metal complexes with anticancer activity, RSC Adv. 4 (63) (2014) 33245–33256, https://doi.org/10.1039/C4RA05355A.
[13] R. Bonsignore, A. Terenzi, A. Spinello, A. Martorana, A. Lauria, A.M. Almerico, B. K. Keppler, G. Barone, G-Quadruplex vs. Duplex-DNA binding of Nickel(II) and Zinc(II) Schiff Base complexes, J. Inorg. Biochem. 161 (2016) 115–121, https://doi.org/10.1016/j.jinorgbio.2016.05.010.
[14] S. Bandeira, J. Gonzalez-Garcia, E. Pensa, T. Albrecht, R. Vilar, A redox-activated G-Quadruplex DNA binder based on a platinum(IV)–Salphen complex, Angew. Chem. Int. Ed. 57 (1) (2018) 310–313, https://doi.org/10.1002/anie.201709968.
[15] C.L. Ruehl, A.H.M. Lim, T. Kench, D.J. Mann, R. Vilar, An octahedral cobalt(III) complex with axial NH $_3$ ligands that templates and selectively Stabilises G-quadruplex DNA, Chem. A Europ. J 25 (41) (2019) 9691–9700, https://doi.org/10.1002/chem.201901569.
[16] M. Gillard, J. Weynand, H. Bonnet, F. Loiseau, A. Decottignies, J. Dejeu, E. Defrancq, B. Elias, Flexible Ru^{II} Schiff Base complexes: G-Quadruplex DNA binding and photo-induced cancer cell death, Chem. A Europ. J 26 (61) (2020) 13849–13860, https://doi.org/10.1002/chem.202001409.
[17] D. Ganci, L. D'Anna, G. Abruscato, M. Le Chevalier, O. Quideau, S. Cataldo, A. Pettignano, S. Rubino, R. Chiarelli, G. Barone, C. Luparello, R. Bonsignore, Harnessing redox reactions for anticancer effects: a copper(II) Schiff Base complex induces apoptosis in HepG2 liver Cancer cells via ROS generation, J. Inorg. Biochem. 270 (2025) 112938, https://doi.org/10.1016/j.jinorgbio.2025.112938.
[18] A.W. Kleij, M. Kuil, M. Lutz, D.M. Tooke, A.L. Spek, Paul Kamer, P.W.N.M. Van Leeuwen, J.N.H. Reek, Supramolecular zinc(II)Salphen motifs: reversible dimerization and templated dimeric structures, Inorg. Chim. Acta 359 (6) (2006) 1807–1814, https://doi.org/10.1016/j.ica.2005.06.069.
[19] A.W. Kleij, J.N.H. Reek, Ligand-template directed assembly: an efficient approach for the supramolecular encapsulation of transition-metal catalysts, Chem. A Europ. J 12 (16) (2006) 4218–4227, https://doi.org/10.1002/chem.200500875.

[20] A.L. Singer, D.A. Atwood, Five-coordinate Salen(tBu) complexes of zinc, Inorg. Chim. Acta 277 (2) (1998) 157–162, https://doi.org/10.1016/s0020-1693(97)06131-8.
[21] E.C. Escudero-Adán, J. Benet-Buchholz, A.W. Kleij, Expedient method for the Transmetalation of Zn(II)-centered Salphen complexes, Inorg. Chem. 46 (18) (2007) 7265–7267, https://doi.org/10.1021/ic701245r.
[22] S. Akine, T. Taniguchi, T. Nabeshima, Novel synthetic approach to Trinuclear 3d-4f complexes: specific exchange of the central metal of a Trinuclear zinc(II) complex of a Tetraoxime ligand with a lanthanide(III) ion, Angew. Chem. Int. Ed. 41 (24) (2002) 4670–4673, https://doi.org/10.1002/anie.200290011.
[23] R. Bonsignore, G. Farine, C. Migliore, G. Gennaro, G. Barone, DNA-binding of zinc (II) and nickel(II) Salphen-like complexes extrapolated at 1 M salt concentration: removing the ionic strength Bias in physiological conditions, J. Inorg. Biochem. 207 (2020) 111064, https://doi.org/10.1016/j.jinorgbio.2020.111064.
[24] P. Thordarson, Determining association constants from titration experiments in supramolecular chemistry, Chem. Soc. Rev. 40 (3) (2011) 1305–1323, https://doi.org/10.1039/c0cs00062k.
[25] A.E. Hargrove, Z. Zhong, J.L. Sessler, E.V. Anslyn, Algorithms for the determination of binding constants and enantiomeric excess in complex host : guest equilibria using optical measurements, New J. Chem. 34 (2) (2010) 348, https://doi.org/10.1039/b9nj00498j.
[26] J.D. McGhee, P.H. Von Hippel, Theoretical aspects of DNA-protein interactions: co-operative and non-co-operative binding of large ligands to a one-dimensional homogeneous lattice, J. Mol. Biol. 86 (2) (1974) 469–489, https://doi.org/10.1016/0022-2836(74)90031-X.
[27] O. Dömötör, F. Binacchi, N. Ribeiro, N. Busto, J. Gonzalez-García, E. Garcia-España, I. Correia, É.A. Enyedy, J. Hamacek, A. Terenzi, N. Basílio, G. Barone, I. Cavaco, T. Biver, How reliable is the evaluation of DNA binding constants? Insights and best practices based on an inter-laboratory fluorescence titration study, Spectrochim. Acta A Mol. Biomol. Spectrosc. 327 (2025) 125354, https://doi.org/10.1016/j.saa.2024.125354.
[28] A. Spinello, A. Magistrato, An omics perspective to the molecular mechanisms of anticancer Metallo-drugs in the computational microscope era, Expert Opin. Drug Discov. (2017) 1–13, https://doi.org/10.1080/17460441.2017.1340272.
[29] M.J. Frisch, G.W. Trucks, H.B. Schlegel, G.E. Scuseria, M.A. Robb, J.R. Cheeseman, G. Scalmani, V. Barone, G.A. Petersson, H. Nakatsuji, Gaussian 16, Revision C.01, Gaussian Inc., 2016. Gassian 16, Revision C.01; Gaussian Inc. 2016.
[30] G.M. Morris, R. Huey, W. Lindstrom, M.F. Sanner, R.K. Belew, D.S. Goodsell, A. J. Olson, AutoDock4 and AutoDockTools4: automated docking with selective receptor flexibility, J. Comput. Chem. 30 (16) (2009) 2785–2791, https://doi.org/10.1002/jcc.21256.
[31] E.F. Pettersen, T.D. Goddard, C.C. Huang, E.C. Meng, G.S. Couch, T.I. Croll, J. H. Morris, T.E. Ferrin, UCSF ChimeraX: structure visualization for researchers, educators, and developers, Protein Sci. 30 (1) (2021) 70–82, https://doi.org/10.1002/pro.3943.